Numerical Simulation of Complex Hypersonic Flows

[1]IST Karachi, [2]Beihang University Beijing, mrmukkarum@yahoo.com

[1]Dr. Mukkarum Husain, [2]Dr. Chun Hian Lee

***Abstract*— Shock/shock and shockwave/ boundary layer interactions are important features of hypersonic flow fields. These features commonly motivate a considerable region of separation followed by reattachment. The pressure loads produced by the shock/shock and shock wave/ boundary layer interactions and the high heating loads encountered at reattachment play a significant role in control surface effectiveness and structural integrity of the hypersonic vehicle. Consequently, CFD tools are under improvement for predicting the details of such complex flows, combined with validating experiments and verifying against basic theoretical relations. In present studies, complex hypersonic flow test cases, namely, compression corner, backward step, and double cone, containing shock/shock and shock wave/ boundary layer interactions are solved by using two different schemes, namely, TVD and low dissipative high resolution artificial compression methods (ACM). Comparison of numerical results against the available experimental data shows that the low dissipative, high resolution ACM provides better results than the TVD scheme. Separation vortex size calculated by low dissipative high resolution ACM method is larger than the size of the separation vortex calculated by the TVD scheme, depicts that the low dissipative high resolution ACM method induces less numerical dissipation and therefore more appropriate for complex shock/shock and shock wave/ boundary layer interactions flows.**

***Index Terms*— Shockwave/Boundary Layer Interaction, TVD, Low Dissipative High Resolution Artificial Compression Method, Compression Corner, Backward Step, Double Cone.**

I. INTRODUCTION

Shock/shock and shockwave/ boundary layer interactions [1-3] are of vital importance for the design of hypersonic flight vehicles. These interactions happen over important components, such as aerodynamic control surfaces and supersonic combustion ramjet (SCRAMjet) intakes, etc. Precise assessment of these interactions severity is essential to ensure satisfactory measures are implemented to counteract the deleterious effects of the shock/shock and shock wave/ boundary layer interactions. Several experimental and theoretical studies dealing with the shock/shock and shock/boundary layer interactions were conducted in the past.

The hypersonic flow around the compression corner [4] with a flow separation upstream from the ramp and involving a multiple shock wave interaction is significantly important for the aero-thermal design of a winged re-entry vehicle. The separated flow over the compression corner involving a multiple shock wave interaction is significantly influences the effectiveness of the control flaps.

Aerothermodynamics loads on the base of re-entry vehicles [5-6] are significant in vehicle drag, heat shield design, payload placement and stability. Considerable uncertainty in predicting the base and wake flow field are often compensated by large factor of safety in the heat shield design. The wake flow field of a hypersonic vehicle has significant influences on vehicle stability, base heating, and optical emissions from non-thrusting vehicles. Even though, the base pressure adds a small proportion to the total drag, the control of vehicle trajectory and attitude requires accurate base pressure estimation.

Flow field around double cone is also very complex [7]. The attached shock from the first cone interacts strongly with the detached shock associated with the second cone. This shock/shock interaction produces a transmitted shock which impinges on the surface of the second cone. Extremely high surface heat transfer rates and pressures generate due to this impingement. The high pressures which result at the cone-cone junction cause the flow to separate in this region. Separation bubble interacts with the inviscid flow field and impacts the strength of the transmitted shock.

Shock/shock and shock/boundary layer interactions can seriously degrade the performance of a hypersonic vehicle. The complexity and the design implications of these phenomena require their quantitative assessment. The precise calculation of supersonic and hypersonic flows put conflicting demands on the formulation of inviscid numerical flux functions. A high speed numerical scheme has to possess enough dissipation to capture strong shocks without developing overshoots and oscillations in the vicinity of the discontinuity and the scheme must also possess numerical dissipation that is much smaller than the physical viscosity to accurately compute boundary layers. The simultaneous satisfaction of these two necessities formulates the computation of viscous hypersonic flows extremely challenging, particularly at the higher Mach numbers where many of the best schemes experience numerical difficulties.

In present studies, two different schemes, namely, TVD [8-11] and low dissipative high resolution artificial compression methods [12] are used to solve complex hypersonic flow test cases, namely, compression corner [13-14], backward step [15-16], and double cone [17-18], containing shock/shock and shock wave/ boundary layer interactions.

II. NUMERICAL ANALYSIS

Numerical analysis has been carried out by using the following two different methods:

Second order Harten-Yee TVD[8-11] scheme for convective part and second order central difference approximation for diffusive part of the governing equations

Forth order ACM [12] for convective part and forth order central difference approximation for diffusive part of the governing equations

Roe's approximate average state is used to calculate eigenvalues and eigenvector matrix [19].

A. Harten-Yee TVD Scheme

The convective flux for Harten-Yee TVD scheme can be cast into the form

$$\frac{\partial F}{\partial x}+\frac{\partial G}{\partial y}+\frac{\partial H}{\partial z}=\frac{1}{\Delta x}\left[\bar{F}_{i+\frac{1}{2}}-\bar{F}_{i-\frac{1}{2}}\right]+\frac{1}{\Delta y}\left[\bar{G}_{j+\frac{1}{2}}-\bar{G}_{j-\frac{1}{2}}\right]+\frac{1}{\Delta z}\left[\bar{H}_{k+\frac{1}{2}}-\bar{H}_{k-\frac{1}{2}}\right] \quad (1)$$

Here,

$$\bar{F}_{i+\frac{1}{2}} = \frac{1}{2}\left[F_i + F_{i+1} + R_{i+\frac{1}{2}}\Phi_{i+\frac{1}{2}}\right] \quad (2)$$

where

$$\Phi^m_{j+\frac{1}{2}} = \sigma\left(a^m_{j+\frac{1}{2}}\right)\left(g^m_{j+1}+g^m_j\right)-\psi\left(a^m_{j+\frac{1}{2}}+\gamma^m_{j+\frac{1}{2}}\right)\alpha^m_{j+\frac{1}{2}} \quad (3)$$

m = 1, 2, 3, 4, 5

$$\psi(z)=\begin{cases}|z| & |z|\geq\delta_1\\ \left(z^2+\delta_1^2\right)/2\delta_1 & |z|<\delta_1\end{cases} \quad (4)$$

$$\boldsymbol{\alpha}_{j+\frac{1}{2}} = \mathrm{R}^{-1}_{j+\frac{1}{2}}\left(U_{j+1}-U_j\right) \quad (5)$$

$$\gamma^m_{j+\frac{1}{2}}=\begin{cases}\left(g^m_{j+1}-g^m_j\right)/\alpha^m_{j+\frac{1}{2}} & For \quad \alpha^m_{j+\frac{1}{2}}\neq 0\\ 0 & For \quad \alpha^m_{j+\frac{1}{2}}=0\end{cases} \quad (6)$$

$$\sigma(z) = \frac{1}{2}\psi(z) + \lambda\beta\,(1-\theta)z^2 \quad (7)$$

For steady state calculation and/or implicit method, we have

$$\sigma(z) = \frac{1}{2}\psi(z) \geq 0 \quad (8)$$

Three limiters are used for Eq. (6) in the present study, namely,

$$g^m_j = \operatorname{minmod}\left(\alpha^m_{j-\frac{1}{2}},\ \alpha^m_{j+\frac{1}{2}}\right) \quad (9)$$

$$g^m_j = \left(\alpha^m_{j+\frac{1}{2}}\alpha^m_{j-\frac{1}{2}}+\left|\alpha^m_{j+\frac{1}{2}}\alpha^m_{j-\frac{1}{2}}\right|\right)\Big/\left(\alpha^m_{j+\frac{1}{2}}+\alpha^m_{j-\frac{1}{2}}\right) \quad (10)$$

$$g^m_j = \operatorname{minmod}\left(2\alpha^m_{j-\frac{1}{2}},\ 2\alpha^m_{j+\frac{1}{2}},\ \frac{1}{2}\left(\alpha^m_{j-\frac{1}{2}}+\alpha^m_{j+\frac{1}{2}}\right)\right) \quad (11)$$

B. Low Dissipative High order ACM

The fundamental idea of these shock-capturing schemes consists of two steps. The first step is a high-order spatial and temporal base scheme. Various standard high-order non dissipative or low dissipative base schemes fit in the current frame work. The second step is the appropriate filter for stability, shocks, contact discontinuities, and fine scale flow structure capturing. Various TVD, positive, WENO, and ENO dissipations, after a slight modification, are appropriate candidates as filters.

1. The base Scheme

Fourth order central differencing used for both convective and diffusion parts of Navier-Stokes equations is given below:

$$\frac{\partial F}{\partial x}=\frac{1}{12\Delta x}\left[F_{i+2,j,k}-8F_{i+1,j,k}+8F_{i-1,j,k}-F_{i-2,j,k}\right] \quad (12)$$

$$\frac{\partial F_v}{\partial x}=\frac{9}{8\Delta x}\left[F_{v\,i+\frac{1}{2},j,k}-F_{v\,i-\frac{1}{2},j,k}\right]-\frac{1}{24\Delta x}\left[F_{v\,i+\frac{3}{2},j,k}-F_{v\,i-\frac{3}{2},j,k}\right] \quad (13)$$

2. The Numerical Flux Filtering Scheme

Non linear dissipation term $\left[\frac{1}{2}R_{i+\frac{1}{2}}\Phi_{i+\frac{1}{2}}\right]$ of Harten-Yee TVD scheme in combination with Harten's switch [20] applied to all characteristic waves as the filter numerical fluxes,

$$\tilde{F}^*_{i+\frac{1}{2}} = k\theta_{i+\frac{1}{2}}\left[\frac{1}{2}R_{i+\frac{1}{2}}\Phi_{i+\frac{1}{2}}\right] \quad (14)$$

The parameter k is a problem dependent. The function $\left[\theta_{i+\frac{1}{2}}\right]$ is the Harten switch. For a general 2m+1 points base scheme, Harten recommended

$$\theta_{i+\frac{1}{2}} = \max\left(\theta_{j-m+1},\ldots\ldots\ldots\ ..,\theta_{j+m}\right) \quad (15)$$

$$\theta = \left(\frac{\left|\left|\alpha_{j+\frac{1}{2}}\right|-\left|\alpha_{j-\frac{1}{2}}\right|\right|}{\left|\alpha_{j+\frac{1}{2}}\right|+\left|\alpha_{j-\frac{1}{2}}\right|}\right)^p \quad (16)$$

For all the numerical examples, we use,

$$\theta_{i+\frac{1}{2}} = \max\left(\theta_j,\theta_{j+1}\right) \quad (17)$$

The new time level is defined as

$$L_f\left(\tilde{F}^*\right)=\frac{1}{\Delta x}\left[\tilde{F}^*_{i+\frac{1}{2},j,k}-\tilde{F}^*_{i-\frac{1}{2},j,k}\right] \quad (18)$$

$$Q^{n+1} = \hat{Q}^{n+1} + \Delta t\, L_f\left(\tilde{F}^*,\tilde{G}^*,\tilde{H}^*\right) \quad (19)$$

III. Test Cases

Three shock/shock and shock wave/ boundary layer interactions hypersonic flow test cases, namely, compression corner [13-14], backward step [15-16], and double cone [17-18] are solved. Descriptions of test cases are given in Table I. Applied boundary conditions are described in figure 1-2 and the associated values are given in Table I. The flows are assumed to be laminar, and the conditions listed in Table I assure that the perfect gas assumption is still valid. Grids used in the three test cases are shown in figures 3-5, respectively.

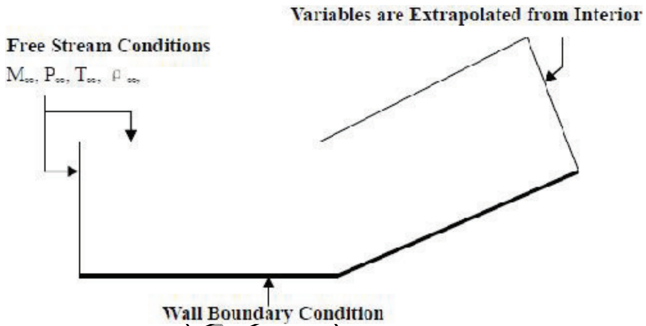

Fig 1: Boundary conditions for 2D cases

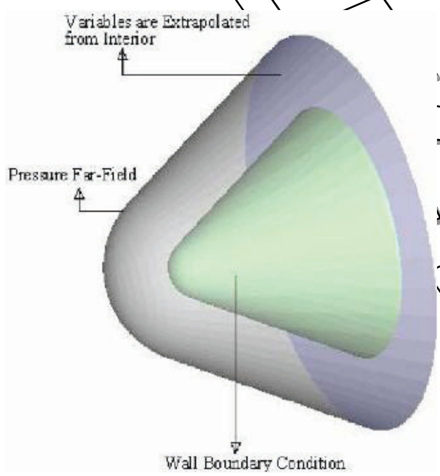

Fig 2: Boundary conditions for 3D case

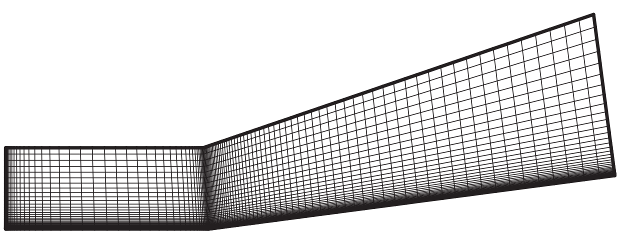

Fig 3: Grid for compression corner

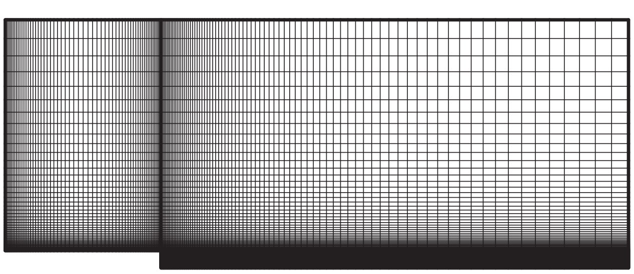

Fig 4: Grid for rearward step

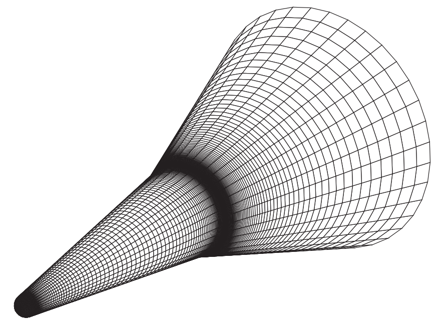

Fig 5: Grid for double cone

TABLE 1
Description of Test Cases

	Test Case 1 (Compression Corner)	Test Case 2 (Rearward Step)	Test Case 3 (Double Cone)
M_∞	6.0	5.0	6.0
Re_{LC}	8×10^5	4.43×10^4	5.73×10^5
T_∞ (K)	57.3	62.96	67.07
$P\infty$(Pascal)	681.156	375.846	673.67
ρ_∞ (kg/m3)	0.04142	0.0208	0.035
Tw (K)	Adiabatic Wall	Adiabatic Wall	Adiabatic Wall
Θ	7.5^0	-90^0	--
L_c (m)	0.04	0.0112522	0.075
R (J/kg-K)	287	287	287
γ	1.4	1.4	1.4
Pr	0.72	0.72	0.72

IV. Results and Discussions

Figures 6-7 shows the comparison between experimental and numerical distributions of pressure coefficient and skin friction coefficient on the wall for compression corner [13-14]. Results for Low Dissipative High Order ACM and Harten-Yee TVD with compressive limiters (eq. 10-11) are closest to experimental results. In particular for ACM scheme, the results are almost identical to the experimental data for both wall pressure and skin friction distribution. Min-mod limiter (eq. 9) provides excess amount of dissipation near corner.

Calculation of extension of the separation vortex is a challenging task for numerical codes. Figure 8 show the separation vortex at the corner using TVD scheme with different limiters and low dissipative high resolution ACM method. The locations of the separation and reattachment point along the compression corner for all schemes are given in Table II. It is noticed from Table II that the TVD scheme with diffusive limiter delays the onset of the separation than other schemes. This is due to the dissipative nature of this limiter, it dissipates the pressure more across the shock. It is also notice that, in the case of low dissipative high resolution ACM method, the size of the separation vortex is larger than the size of the separation vortex calculated by TVD scheme with different limiters, indicating that the numerical dissipation of low dissipative high resolution ACM method is indeed lower than TVD scheme.

Figure 9 shows the comparison between experimental and numerical distributions of pressure ratio on the wall for backward step [15-16]. In this test case, Harten-Yee TVD scheme with all three different limiters is failed to predict base pressure and pressure down stream the step. Result for Low Dissipative High Order ACM is in reasonably good agreement with experimental results. But the wall pressure starts to deviate from the experimental results and becomes worsened further downstream, demonstrate that the wake flow region is difficult to capture due to the highly separated and reverse flows that complicate flow field predictions.

Figures 10-11 show the small and the large separation vortices at the corner of rearward step by using TVD scheme and low dissipative high resolution ACM method. Table III summarizes the length of separation vortices calculated by both schemes. It is noticed from Table III that in the case of low dissipative high resolution ACM method, the size of the separation vortex is larger than the size of the separation vortex calculated by TVD scheme, revealing that low dissipative high resolution ACM method scheme induces less numerical dissipation.

Finally, hypersonic flow around double cone is solved. Figure 12 shows the comparison between experimental and numerical distributions of pressure on the wall of double cone [17-18]. Results for low dissipative high order ACM are closest to experimental results. TVD provides excess amount of dissipation near the corner.

Figure 13 show the separation vortex at the cone–flare region of double cone by using TVD scheme and low dissipative high resolution ACM method, respectively. The location of the separation and reattachment point for both schemes are given in Table IV. It is observed that in the case of low dissipative high resolution ACM method, the size of the separation vortex is larger than the size of the separation vortex calculated by TVD scheme, indicating that the numerical dissipation of low dissipative high resolution ACM method is indeed lower than TVD scheme.

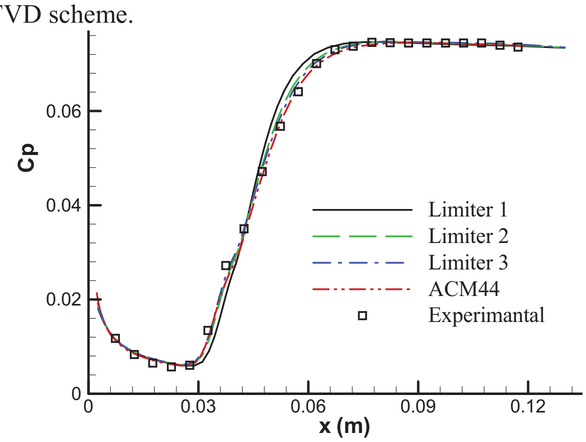

Fig 6: Comparison of Pressure Coefficient along wall of Compression Corner

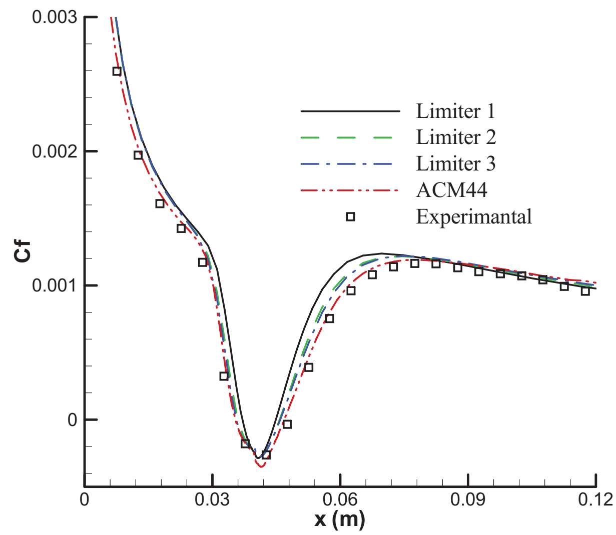

Fig 7: Comparison of Skin Friction Coefficient along wall of Compression Corner

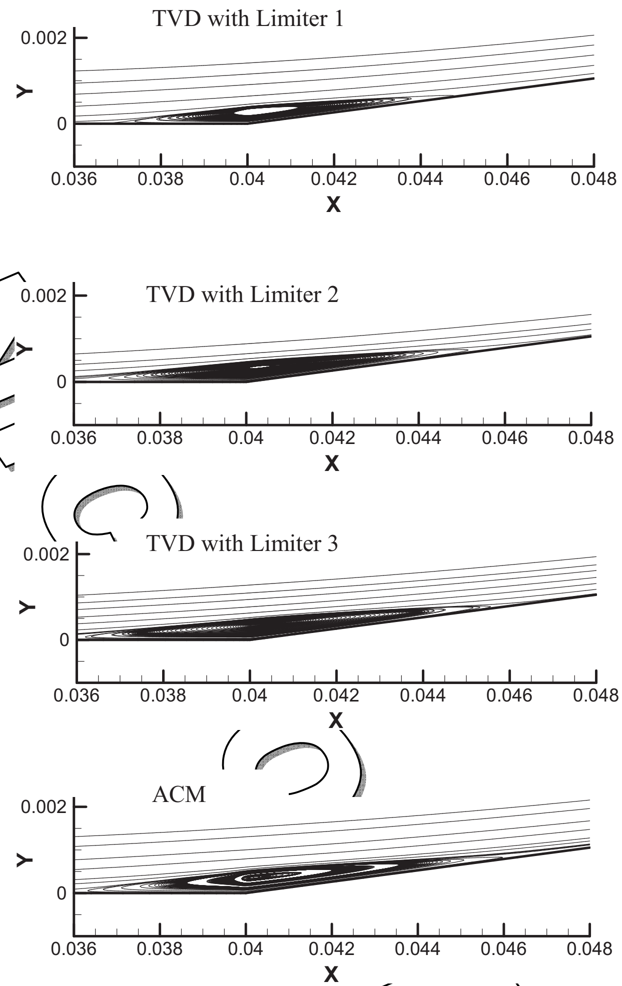

Fig 8: Separation Vortex at Compression Corner

TABLE II
LOCATION OF SEPARATION AND REATTACHMENT FOR COMPRESSION CORNER

Scheme	Separation Point (m)	Reattachment Point (m)
TVD Limiter 1	0.0373	0.0437
TVD Limiter 2	0.0368	0.0450
TVD Limiter 3	0.0363	0.0455
Low Dissipative High Resolution ACM	0.0363	0.0460

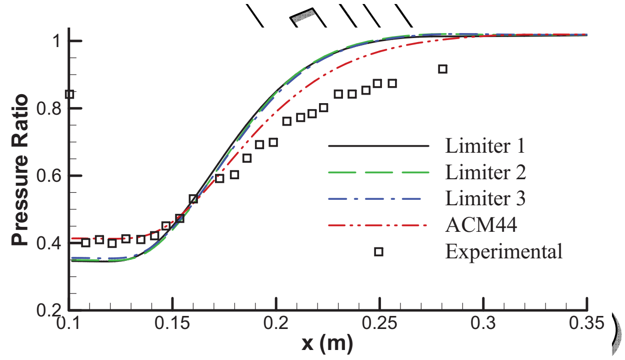

Fig 9: Comparison of Pressure ratio along wall of Rearward Step

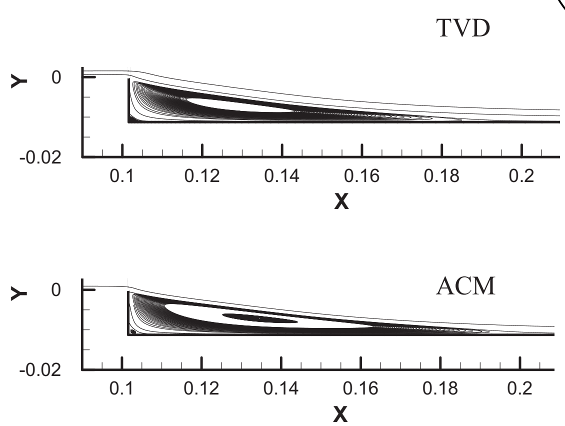

Fig 10: Primary Vortex at Corner of Rearward Step

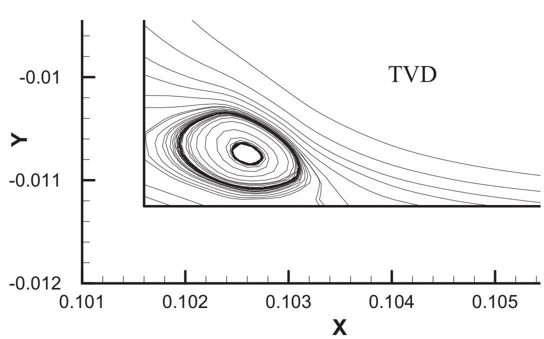

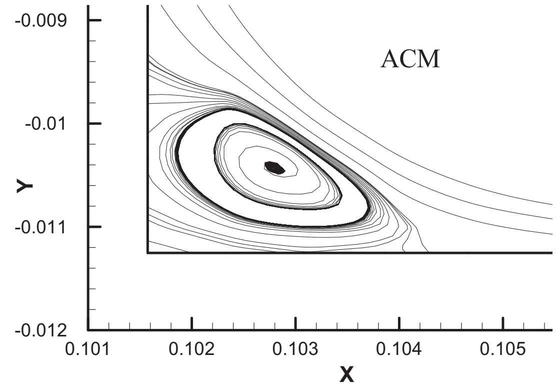

Fig 11: Small Vortex at Corner of Rearward Step

TABLE III
Vortex Length at Rearward Step by Different Scheme

Scheme	Secondary Vortex Length (m)	Primary Vortex Length (m)
TVD	0.0016	0.0834
Low Dissipative High Resolution ACM	0.0026	0.0904

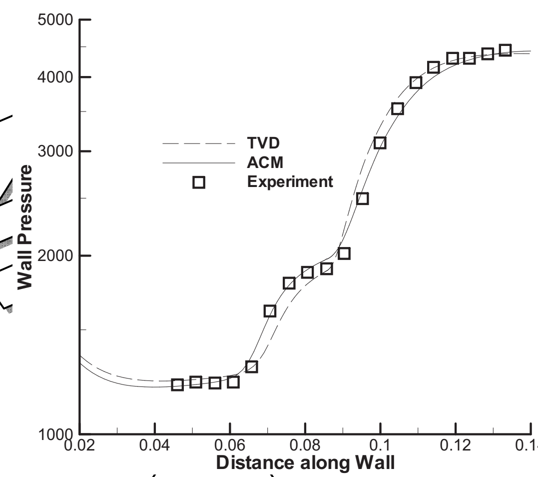

Fig 12: Comparison of Pressure along wall of Double Cone

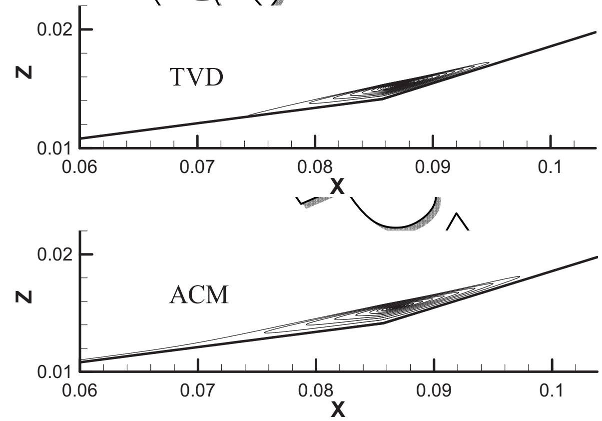

Fig 13: Separation Vortex at Cone–Flare Region

TABLE IV
Location of Separation and Reattachment for Double Cone

Scheme	Separation Point (m)	Reattachment Point (m)
TVD	0.079	0.095
Low Dissipative High Resolution ACM	0.076	0.097

V. Conclusion

Comparison of numerical results against available experimental data illustrate that the low dissipative high resolution ACM provide better results than the TVD scheme. It is also observed that the size of the separation vortex calculated by low dissipative high resolution ACM method is larger than the size of the separation vortex calculated by TVD scheme, revealing that the numerical dissipation of low dissipative high resolution ACM method is indeed lower than the TVD scheme. Present studies depicts that it is appropriate to use low dissipative high resolution ACM for accurate assessment of shock/shock and shock wave/ boundary layer interactions severity to counteract its deleterious effects.

Acknowledgment

The first author would like to acknowledge the financial support from the Higher Education Commission (HEC) Pakistan.

References

[1] Krishnendu Sinha, Graham V, "Candler. Grid Sensitivity of Detached eddy simulation of a Mach 16 Re-entry Configuration," 45th AIAA Aerospace Sciences Meeting and Exhibit 8 - 11 January 2007, Reno, Nevada, AIAA 2007-1115.

[2] George R. Inger, James N. Moss, "Comparison of Navier–Stokes and Direct Simulation Monte Carlo Predictions with Separation," AIAA Journal Vol. 45, No. 8, August 2007.

[3] R. C. Mehta, "Three-Dimensional Inviscid Flowfield Computation over Various Reentry Configurations," 45th AIAA Aerospace Sciences Meeting and Exhibit 8 - 11 January 2007, Reno, Nevada, AIAA 2007-133., 2007

[4] Laurie M. Brown, Russell R. Boyce, Neil Mudford and Sean O'Byrne, "Intrinsic Three-Dimensionality of Laminar Hypersonic Shock Wave/Boundary Layer Interactions," 16th AIAA/DLR/DGLR International Space Planes and Hypersonic Systems and Technologies Conferenc AIAA 2009-7205, 2009.

[5] Datta V. Gaitonde, "The Mean Flowfield Structure of a Supersonic Three Dimensional Base Flow," 46th AIAA Aerospace Sciences Meeting and Exhibit 7 - 10 January 2008, Reno, Nevada, AIAA 2008-573, 2008.

[6] Soshi Kawai, Kozo Fujii, "Time-Series and Time-Averaged Characteristics of Subsonic to Supersonic Base Flows," AIAA Journal, Vol. 45, No. 1, January 2007.

[7] Robert W. Tramel , Robert H. Nichols, Pieter G. Buning, "Addition of Improved Shock-Capturing Schemes to OVERFLOW 2.1," 19th AIAA Computational Fluid Dynamics 22 - 25 June 2009, San Antonio, Texas, AIAA 2009-3988, 2009.

[8] A Harten, "On a Class of High Resolution Total-Variation-Stable Finite Difference Schemes," SIAM J. Numerical Anal., vol. 21, 1984.

[9] A Harten, "High Resolution Schemes for Hyperbolic Conservation Laws," J. Computational Phys., vol.49, pp. 357-393, 1983.

[10] Yee, H.C., G. H. Klopfer, and J. -L. Montagne, "High-Resolution Shock-Capturing Schemes for Invicid and Viscous Hypersonic Flows," J. Comput. Phys., vol.88, pp. 31-61, 1990.

[11] Yee, H.C., "Upwind and Symmetric Shock-Capturing Schemes," NASA TM-89464, 1987.

[12] Yee, H.C., N. D. Sandham, and M. J. Djomehri, "Low Dissipative High Order Shock Capturing Methods Using Characteristic-Based Filters," J. Comput. Phys., vol.150, pp.199-238, 1999.

[13] Hoffmann, K. A. Dietiker, J. F., and Chiang, S. T., "Student Guide to CFD," Engineering Education Systems, Volume II, 2001.

[14] Kamran R. Q., "Numerical Simulation of High Speed Vehicle using High Resolution, High-Order, and Low Dissipative Scheme," PhD thesis, Beihang University, Beijing, China, 2008.

[15] Howard, and E. Smith, "The Flow Field and Heat Transfer Downstream of a Rearward Facing Step in Supersonic Flow[R]," Aerospace Research Laboratory, ARL 67-0056, 1967.

[16] R. H. Nichols, J. R. Maus, G. A. Molvik, "Calculation of High Speed Base Flow," AIAA-92-2679-CP, 1992.

[17] W. Dieudonne, H. L. Boerrigter, J. M. Charbonnier, "Hypersonic Flow on a Blunted Cone Flare and in the VKI-H3 Mach 6 wind tunnel," Von Karman Institute, Belgium, 1996.

[18] R. Savino, D. Paterna, "Blunted Cone-Flare in Hypersonic Flow". Computers & Fluids 34 (2005) 859–875, 2005.

[19] P. L. Roe, "Approximate Riemann Solvers, Parameter Vectors, and Difference Schemes," J. Comput. Phys., vol.43, pp.357, 1981.

[20] Harten A, "The Artificial Compression Method for Computation of Shocks and Contact Discontinuities, III Self-Adjusting Hybrid Schemes," Math Comp., 32:363-389, 1978.